Integrative Biology

Quantitative biosciences from nano to macro

www.rsc.org/ibiology

Volume 1 | Number 2 | February 2009 | Pages 133–224

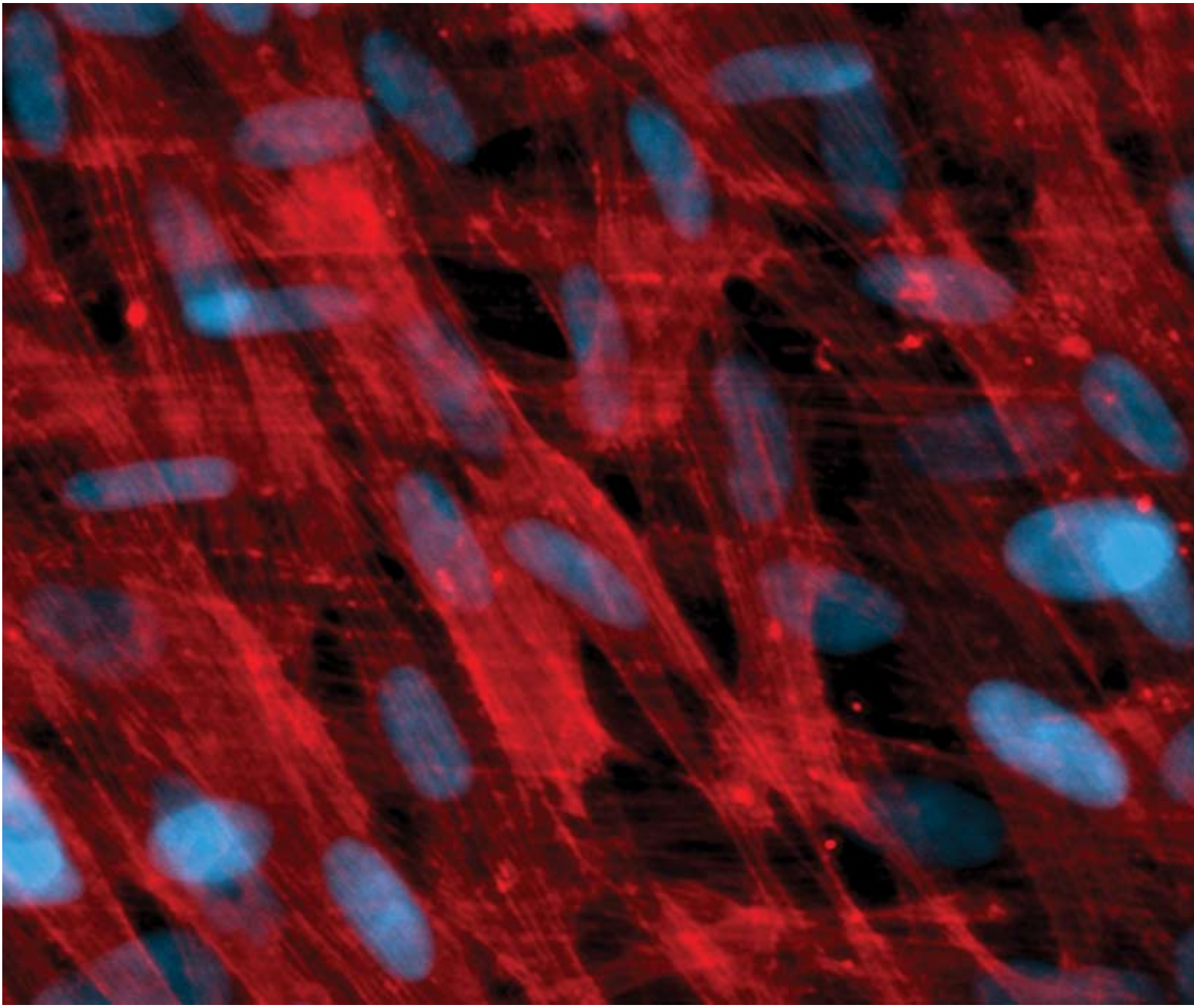

ISSN 1757-9694

RSC Publishing

Nicolau *et al.*
Modelling protein motors

Auger *et al.*
3D Self-orientation of cells & ECM

1757-9694(2009)1:2;1-S

Surface topography induces 3D self-orientation of cells and extracellular matrix resulting in improved tissue function†

Maxime D. Guillemette,[abc] Bo Cui,[c] Emmanuel Roy,[c] Robert Gauvin,[ab] Claude J. Giasson,[d] Mandy B. Esch,[e] Patrick Carrier,[a] Alexandre Deschambeault,[a] Michel Dumoulin,[c] Mehmet Toner,[f] Lucie Germain,[ab] Teodor Veres[bc] and Francois A. Auger*[ab]

Received 24th November 2008, Accepted 23rd December 2008
First published as an Advance Article on the web 15th January 2009
DOI: 10.1039/b820208g

The organization of cells and extracellular matrix (ECM) in native tissues plays a crucial role in their functionality. However, in tissue engineering, cells and ECM are randomly distributed within a scaffold. Thus, the production of engineered-tissue with complex 3D organization remains a challenge. In the present study, we used contact guidance to control the interactions between the material topography, the cells and the ECM for three different tissues, namely vascular media, corneal stroma and dermal tissue. Using a specific surface topography on an elastomeric material, we observed the orientation of a first cell layer along the patterns in the material. Orientation of the first cell layer translates into a physical cue that induces the second cell layer to follow a physiologically consistent orientation mimicking the structure of the native tissue. Furthermore, secreted ECM followed cell orientation in every layer, resulting in an oriented self-assembled tissue sheet. These self-assembled tissue sheets were then used to create 3 different structured engineered-tissue: cornea, vascular media and dermis. We showed that functionality of such structured engineered-tissue was increased when compared to the same qnon-structured tissue. Dermal tissues were used as a negative control in response to surface topography since native dermal fibroblasts are not preferentially oriented *in vivo*. Non-structured surfaces were also used to produce randomly oriented tissue sheets to evaluate the impact of tissue orientation on functional output. This novel approach for the production of more complex 3D tissues would be useful for clinical purposes and for *in vitro* physiological tissue model to better understand long standing questions in biology.

[a] *LOEX, Centre de recherche (FRSQ) du CHA de Québec, Quebec City, PQ, Canada*
[b] *Department of Surgery, Faculty of Medicine, Laval University, Quebec City, PQ, Canada. E-mail: francois.auger@chg.ulaval.ca*
[c] *Industrial Materials Institute, National Research Council, Boucherville, PQ, Canada*
[d] *School of Optometry, Research Unit in Ophthalmology, Montreal University, Montreal, PQ, Canada*
[e] *Biomedical Engineering Department, Cornell University, Ithaca, NY, USA*
[f] *Center for Engineering in Medicine and Surgical Services, Massachusetts General Hospital, Harvard Medical School, and Shriners Hospital for Children, Boston, MA, USA*

† Electronic supplementary information (ESI) available: Video of time lapse microscopy images. See DOI: 10.1039/b820208g

Introduction

One of the pivotal challenges of tissue engineering is to obtain truly functional tissues and organs. Complex structural organization in the human body leads to appropriate functionality of organs. The various human connective tissues are composed of cells and ECM and their 3D structure is adapted to their functions, either biological or mechanical. The transparency necessary for the optical function of the cornea is dependent on the unique spatial organization of the corneal stroma.[1] The structural arrangements of blood vessels favor the contraction of smooth muscle cells[2] and their compliance. In skin, the general orientation of the collagen

Insight, innovation, integration

In the present study, we used contact guidance to control the interactions between material topography, cells and the extracellular matrix (ECM). These experiments led to the original observation that normal human cells from three different tissues, after being provided the same initial orientation guidance from micropatterned biomaterials, have the capacity to subsequently generate multiple layers, in which cells and the ECM spontaneously organize in patterns consistent with the tissue of origin. This technique can be used as a powerful *in vitro* model to investigate the biological mechanisms of spontaneous tissue self-patterning. It can also lead to tissue-engineered substitutes, in which normal human cells will spontaneously fall into the alignment patterns necessary for optimization of their physiological function.

is used by plastic surgeons to minimize scarring in wound healing.[3,4] The complex internal architecture of the corneal stroma presents a 60 degree shift in the alignment of collagen fibers of consecutive planes or lamellae. Tissue-engineered substitutes are typically produced by embedding cells in scaffolds or synthetic materials.[5] This approach often results in poorly controlled cellular and ECM alignment.

The self-assembly method[6,7] allows for the creation of tissue-engineered constructs without the use of any exogenous scaffold material. Using this method, the cells and cell-secreted extracellular matrix (csECM) form complex sheets with an overall random orientation when cultured on a flat substrate. To orient cells and collagen in a preferential direction, some groups have used strain,[8] magnetic[9] or electric[10] fields. Our group succeeded in orienting cells and csECM in a favored direction by using mechanical loading of fibroblastic and smooth muscle cell sheets obtained by the self-assembly approach.[11,12] However, these methods allow for the creation of tissues oriented in a single preferred direction but do not result in different orientations of cells and ECM within one tissue construct. Surface micropatterning[13] has been used in order to study cell distribution and organization utilizing biochemical cues. However, the lack of cell structure stability[14] of the created motifs does not allow for long-term tissue engineering studies. In contact guidance,[15–19] a rigid physical profile imprinted on a material defines how cells interact with each other and align themselves. No study, however, has shown how the substrate surface topography would direct the orientation of csECM.

The present study evaluates a more simple approach related not only to surface topography but cell–ECM and cell–cell interactions occurring naturally within the cultured tissue. We used a thermoplastic elastomer (TPE) engraved with a grating period of 4 μm to observe corneal stromal, dermal and smooth muscle cells aligned along the surface topography. Since cells aligned on the grooves, cell–cell interactions were possible over the entire sample, leading to ECM secretion and organization following cell orientation. We also observed that the second cell–ECM layer produced is highly organized to a level found only in their physiological tissue counterparts and finally, that the functionality of such structured engineered-tissue is increased compared to the same non-structured tissue. Those results highlight how the final spatial organization of our tissue obtained by the self-assembly method of tissue engineering is dependent on the nature and properties of the cells originating from the very tissue we strive to reproduce.

Experimental

Substrate fabrication

Si molds from 2 μm to 10 μm period used for the hot embossing process were fabricated by standard photolithography. Trenches were etched by reactive ion etching (RIE) (PlasmaLab 80 Plus, Oxford Instruments, UK) using a mixture of gas of 20 sccm CF_4 and 2 sccm O_2 at 10 mTorr and 100 W. Trench depth was approximately 1 μm. 1 μm period molds were fabricated by DUV lithography and RIE with a linewidth and depth of 0.5 μm. Microstructured PS replication were created by hot embossing (EVG520 system) of PS pellets (120 kg mol^{-1}) distributed evenly over an area of about 50 cm^2 on top of the Si mold. After heating to 160 °C, a force of 1500 N was applied for 2 min under a vacuum below 1 Torr, followed by the application of the final force of 10 000 N for 5 min. Both the mold and the flat wafer were treated with anti-adhesion silane prior to the embossing process in order to facilitate demolding. Microstructured TPE were created by heating the polymer to 170 °C on the mold, no pressure or vacuum was necessary. All substrates were treated with oxygen plasma at 100 W, 20 sccm O_2 and 10 mTorr for 20 s.

Electron microscopy analysis

For scanning electron microscopy (SEM), high-resolution images of the Si molds and TPE substrates were obtained using a Hitachi S4800 field-emission scanning electron microscope. For transmission electron microscopy (TEM), samples were fixed in 2.5% gluteraldehyde and processed for electron microscopy as previously described.[20]

Cell and tissue culture

Human stromal corneal fibroblasts were isolated and cultured from post-mortem donor corneas unsuitable for transplantation (Banque nationale d'yeux du Centre hospitalier universitaire de Québec) as described previously.[21] Cells were cultured in Dulbecco-Vogt modification of Eagle's medium (DMEM, Invitrogen, Burlington, ON, Canada) supplemented with 10% fetal calf serum (Hyclone, Logan, UT), 100 IU mL^{-1} penicillin G (Sigma, Oakville, Ontario, Canada) and 25 μg mL^{-1} gentamicin (Schering Canada, Pointe-Claire, Québec, Canada) containing 50 μg mL^{-1} of fresh ascorbic acid (Sigma). Human skin fibroblasts were obtained from the dermis of adult breast skin and cultured as described previously.[20] Cells were grown under 8% CO_2 at 37 °C, and the culture medium was changed three times a week. Fibroblast sheets from human cornea (100 microstructured samples and 25 controls) or dermis (32 microstructured samples and 10 controls) were respectively obtained after 60 and 28 days of culture in the presence of 50 μg mL^{-1} of sodium ascorbate (Sigma). SMC isolation was done as described previously.[7] Smooth muscle cell (SMC) sheets on microstructured samples ($n = 23$) and control ($n = 17$) were obtained following 13 days of culture in the presence of 50 μg mL^{-1} of ascorbate (Sigma).

Human tissue-engineered corneas cultured on microstructured ($n = 5$) and on control($n = 5$) substrates were obtained using the self-assembly approach as described previously.[22] Microstructured corneal stroma sheets were stacked following their internal orientation by shifting the cell sheet 60 degree from the previous one. Then epithelial cells were seeded following our usual approach.[22] Tissue engineered vascular media (TEVM) were produced using our previously described method[7] on microstructured ($n = 3$) or control substrates ($n = 3$). For TEVM grown on microstructured substrates, cell sheets were rolled circumferentially on the mandrel. Dermal fibroblast sheets were produced on microstructured ($n = 4$) and control substrates ($n = 4$) following the self-assembly approach.

Histology and immunochemistry

To stain type I collagen, the whole thickness of the cultured tissue was fixed in formol 3.7% for 1 h and washed three times for 10 min before and after the fixation in phosphate buffered saline (PBS). The primary antibody was a rabbit monoclonal anti-human collagen I (Cedarlane, Burlington, ON, Canada). A chicken anti-rabbit conjugated with Alexa 594 (Molecular Probes, Eugene, OR, USA) was used against the primary antibody. Tissues were incubated with antibodies, diluted in PBS containing 1% bovine serum albumin (Sigma), at 4 °C overnight (primary antibody) and washed three times for 10 min in PBS before incubation at 4 °C overnight in the dark (conjugated antibody). To stain actin filaments, tissues were fixed in methanol for 10 min and washed three times for 2 min before and after the fixation in phosphate buffered saline (PBS). The primary antibody was either a rabbit monoclonal anti-actin (Cedarlane, Burlington, ON, Canada) for corneal and dermal fibroblasts or a rabbit monoclonal anti-smooth muscle actin (DakoCytomation, Mississauga, ON, Canada) for SMC. A goat anti-rabbit conjugated with Alexa 594 (Molecular Probes, Eugene, OR, USA) was used against all primary antibodies. Tissues were incubated with antibodies, diluted in PBS containing 1% bovine serum albumin (Sigma) for 30 min (primary antibody) and washed three times for 10 min in PBS before 30 min incubation in the dark (conjugated antibody). Cells nuclei were labeled with Hoechst reagent 33 258 (Sigma) following immunofluorescence staining for all procedures. Immunofluorescence was measured using a Nikon Eclipse E800 confocal microscope combined with Nikon D-Eclipse C1 system or a time lapse microscope combined with ORCA-ER Hamamatsu system.

Angle shift analysis

Immunofluorescence imaging of five different sections of each type of tissue showing actin filaments were processed for angle shift measurements. Twenty five measurements per section were acquired using the SimplePCI® software. Angle shift was defined as the angle between the major axis of the actin filaments of cells from the bottom layer compared with the axis of cell from the top layer. Data from the same cell type were pooled since no statistical difference was observed between samples of a same group. Angle shift data were analyzed using the Minitab® Software. Normality was established using the Anderson-Darling test with a standard $p < 0.05$. Results are expressed as mean ± standard deviation on normal distribution plots of angle shift measurement for each cell type. Comparison of angle shift values between the different cell types was performed using an analysis of variance (ANOVA) general linear model. Statistical significance was established using a standard $p < 0.05$.

Mechanical testing and analysis

Mechanical characterization of the engineered-tissues was assessed by ring testing in the case of the TEVM and by uniaxial tensile test for the dermal fibroblast sheets. The ring test was performed on 5 mm sections of the TEVM, loaded onto a pair of hooks mounted on a tensile apparatus (MTS Systems Corporation, Eden Prairie, MN). Samples were strained at a constant rate (0.2 mm s^{-1}) until failure. Uniaxial tensile test was performed on a bone shape sample cut into a dermal fibroblast sheet (gauge length of 3 mm × 10 mm) mounted on the previously stated apparatus and using the same loading conditions. Engineering stress and strain was used to determine the mechanical properties of both samples.

Measurement of transmittance

Indirect transmittance was measured using a scanning double beam Varian UV-vis-IR (Cary 5000) spectrophotometer (Mulgrave, Australia) with the integrating sphere (radius: 110 mm) of the internal diffuse reflectance accessory. Reconstructed tissues were immersed in a phosphate buffered saline (PBS) solution and placed in a quartz chamber especially designed for spectrophotometric measurements. Baseline transmittance was measured using the chamber filled with saline.

Results and discussion

Substrate fabrication

The production of living tissue-engineered substitutes by the self-assembly approach requires adequate cell proliferation, ECM secretion and organization so that the resulting tissue sheets are strong enough to be manipulated (Fig. 1a). Thus, it demands culturing cells on an optimal surface such as polystyrene (PS), which is currently the most widely used synthetic polymeric material for cell culture. We took advantage of emerging microfabrication technologies that allow for a precise and rapid microstructuration of a TPE substrate: (styrene)–(ethylene/butylene)–(styrene) (SEBS). We report here a high-throughput thermal replication method for such a polymer, where embossing experiments have been done over large surfaces without pressure and vacuum assistance within an overall cycle time of 180 s.

In order to evaluate how efficient this polymer is for cell culture, we compared it to microfabricated PS that was used as a control for cell proliferation and ECM secretion. As the results for PS and SEBS were very similar (data not shown) in the initial experiments, we used SEBS substrates throughout the remainder of the study since it is easier to mold than PS. The SEBS substrates were structured by hot embossing to form gratings with different periods ranging from 1 μm to 10 μm and wall thicknesses between 500 nm and 5 μm using Si molds created with UV photolithography (Fig. 1b) followed by a hot embossing step (Fig. 1c). SEBS samples were then treated with oxygen plasma (Fig. 1d) prior to sterilization using the standard ethylene oxide gas technique. Atomic force microscopy (AFM) (Fig. 1e) and scanning electron microscopy (SEM) (Fig. 1f) imaging showed a high fidelity replication of the Si mold architecture in the SEBS substrate. These substrates can be created over large surface areas, thus allowing the production of tissue-engineered vascular media (TEVM), tissue-engineered cornea or tissue-engineered skin of adequate size.

This model differs from previous microstructured platform made of Si wafer[23] or polydimethylsiloxane (PDMS)[24] mainly because it allows for the production of oriented csECM on

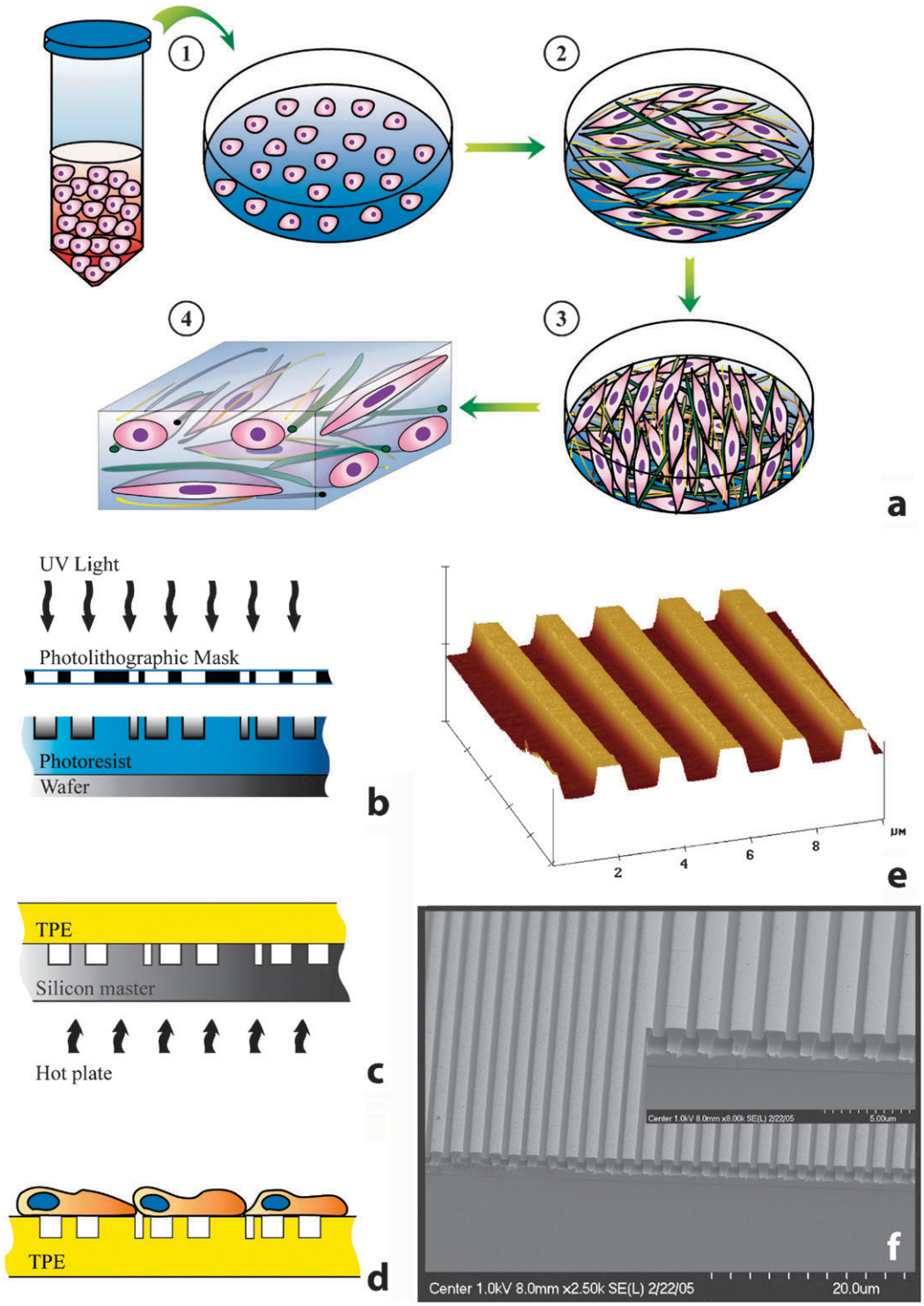

Fig. 1 Schematic illustration of the self-assembly method (**a**). Cells are plated in a single cell seeding procedure (**a1**) and their number increase through cell proliferation. They are cultured in the presence of sodium ascorbate to stimulate ECM synthesis (**a2**). Cells are maintained in culture until their neosynthesized ECM proteins have self-assembled into an adherent living tissue sheet comprised of cells and ECM (**a3**). The tissue sheet can be manipulated with tweezers and do not contain any exogenous biomaterials, only cells and their secreted ECM as shown in a magnified view illustration (**a4**). Process for the fabrication of the microstructured TPE substrates. The master was fabricated in Si wafer by standard photolithography. Etching of the gratings into the Si master was made by Cr deposition, liftoff of the photoresist and reactive ion etching using CF_4–O_2 gas with Cr as a mask (**b**). After an etching procedure, the silicon master is used to replicate the same structure in TPE. A flat piece of TPE is placed on the master and then heated to allow the TPE to flow in the gratings of the silicon master (**c**). After an oxygen plasma treatment and sterilization, TPE substrates are used for cell culture (**d**), samples are placed in Petri dishes before cell seeding at step (**a1**) to induce cell orientation in culture instead of using regular Petri dishes that result in randomly distributed cells in culture. AFM image of the silicon master after the etching procedure (**e**). SEM image of a microstructured substrate replica created by hot embossing (**f**).

microstructured SEBS substrates. This material is excellent for cell culture since it is comparable to microstructured PS (Guillemette *et al*. unpublished results). In fact, the selected TPE material is a block copolymer where nanophase separation occurs. For specific SEBS plastics, such as the ones used in our experiments, the styrene content is nearly equal to 10–12%. In addition, the self-assembling of styrene blocks leads to nanometric cluster domains of polystyrene which is a suitable material for cell culture. SEBS mechanical properties offer additional advantages over rigid PS, such as a Young modulus of −1.14 MP and a 700–1000% stretchable capacity. Additionally, as commercially available PS culture dishes, SEBS material can be treated with oxygen plasma and also be sterilized by standard ethylene oxide gas technique.

Cell organization on microstructured substrates

We first analyzed how cells reacted to the controlled physical environment to find parameters favoring the orientation of cells that will then result in the secretion of organized extracellular matrix. We observed that a range of grating periods from 1 μm to 4 μm was optimal to align various human cell types such as smooth muscle cells, corneal and dermal fibroblasts (data not shown). In order to study how quickly cells adhered and aligned on the SEBS grating, time lapse microscopy analyses were performed (Supporting video 1†). Cells readily aligned after plating on the microstructured substrates and cell movement occurred parallel to the axis of the grating. Moreover, after cell division, daughter cells aligned on the microstructured substrate in this same parallel direction. Immunofluorescence of actin filaments revealed that human smooth muscle cells, corneal and dermal fibroblasts aligned in the direction of the grating as compared to the random organization observed on flat substrates used as controls (Fig. 2).

Corneal fibroblasts reached confluence within 6 days, after which they began to grow on top of the aligned first cell layer (Fig. 2e). The second corneal fibroblast layer was observed at day 9. It formed at an angle shift of 53 ± 8 degree (Fig. 2s) relative to the first corneal fibroblast layer. Accordingly, the second smooth muscle cell layer formed at day 13 (Fig. 2l) with a 39 ± 4 degree (Fig. 2t) angle shift from the first layer. In the first layer, dermal fibroblasts aligned in the direction of the gratings (Fig. 2q) whereas the second layer was not oriented (Fig. 2r and Fig. 2u). Although some very local pattern could be noted, no particular orientation over a significant surface area was observed for the first layer of the different cell types cultured on the control substrates, nor in the subsequent layers appearing after confluence. Thus, human cells seeded on microstructured substrates formed 3D tissues with alignment resembling that of their corresponding native tissues.

It has been shown that cells orient on a nanostructured surface by inducing reorganization of the cytoskeleton components, including actin filaments.[25] However, most model found in the literature used groove patterns that allow cells to penetrate within each groove. In the model presented here, cell orientation is possible since in the first layer cells proliferate and divide following the longitudinal microstructured SEBS and not because they are being forced into a groove without being able to exit. This phenomenon is important to maintain the cell–cell and cell–ECM interactions[26] and permits the alignment of the cells and csECM over large surface area. Moreover, the realignment of daughter cells in the longitudinal direction of the ridges, after cell division occurred, allowed the preservation of cell orientation with cell growth.

ECM organization on microstructured substrates

In order to follow the orientation of the ECM deposited by the cells, immunostainings of type I collagen, one of the main components of the ECM produced by human smooth muscle cells, dermal and corneal fibroblasts were performed. We used self-assembled tissue sheets coming from a single cell seeding as described in Fig. 1a. It has been previously demonstrated that ECM follow cell orientation. No preferred orientation was noticed in the control tissue sheets of all cell types cultured on flat substrates (Fig. 3). In contrast, stack render images of corneal fibroblasts (Fig. 3a) and smooth muscle csECM (Fig. 3b) grown on microstructured SEBS showed a highly organized internal structure. For both corneal fibroblast and smooth muscle cell tissue sheets, the ECM alignment is in keeping with the angle measured from cell alignments in Fig. 2 consistent with the known parallel alignment of cell and ECM. Confocal imaging of immunostained sections of type I collagen in the dermal fibroblast sheets (Fig. 3c) cultured on microstructured or flat SEBS were analyzed to observe fiber orientation. Dermal sheets cultured on flat substrates showed no preferred orientation. In contrast to corneal fibroblasts and smooth muscle cells, when dermal fibroblasts were cultured on microstructured substrates, csECM exhibited only a tendency to orient in the first layer, and no evidence of alignment was observed in the second layer.

The orientation of csECM in the corneal stroma was further defined by electron microscopy with SEM imaging of the corneal stroma in a slanted cross-section in order to illustrate the different collagen layers within a tissue sheet. In the control sheets produced over flat substrates, the upper plane did not present preferential fiber alignment (Fig. 4a). In the lower layers of csECM, the collagen fibers displayed no preferential orientation either (Fig. 4a, inset). In contrast, specific alignment of the csECM was observed within corneal fibroblast sheets grown on microstructured SEBS. A parallel csECM alignment of the top layer was visualized by SEM imaging (Fig. 4b) indicating a well defined fiber architecture. Moreover, the 60 degree angle shift between two consecutive layers was apparent at higher magnification (Fig. 4b, inset).

A random distribution of collagen fibers cut in a perpendicular (dots) or longitudinal (lines) fashion was observed in control sheets analyzed using transmission electron microscopy (TEM) (Fig. 4c). In contrast, regularly spaced rows of lines alternating with dots were observed in the microstructured SEBS samples (Fig. 4d), indicating that the stromal sheets comprised layers of aligned collagen fibers shifting from plane to plane. The typical collagen fiber striation pattern was observed at higher magnification of TEM images in both control (Fig. 4e) and microstructured SEBS (Fig. 4f), indicating that collagen was present in csECM. These results indicate that the tissue resulting from the culture of corneal

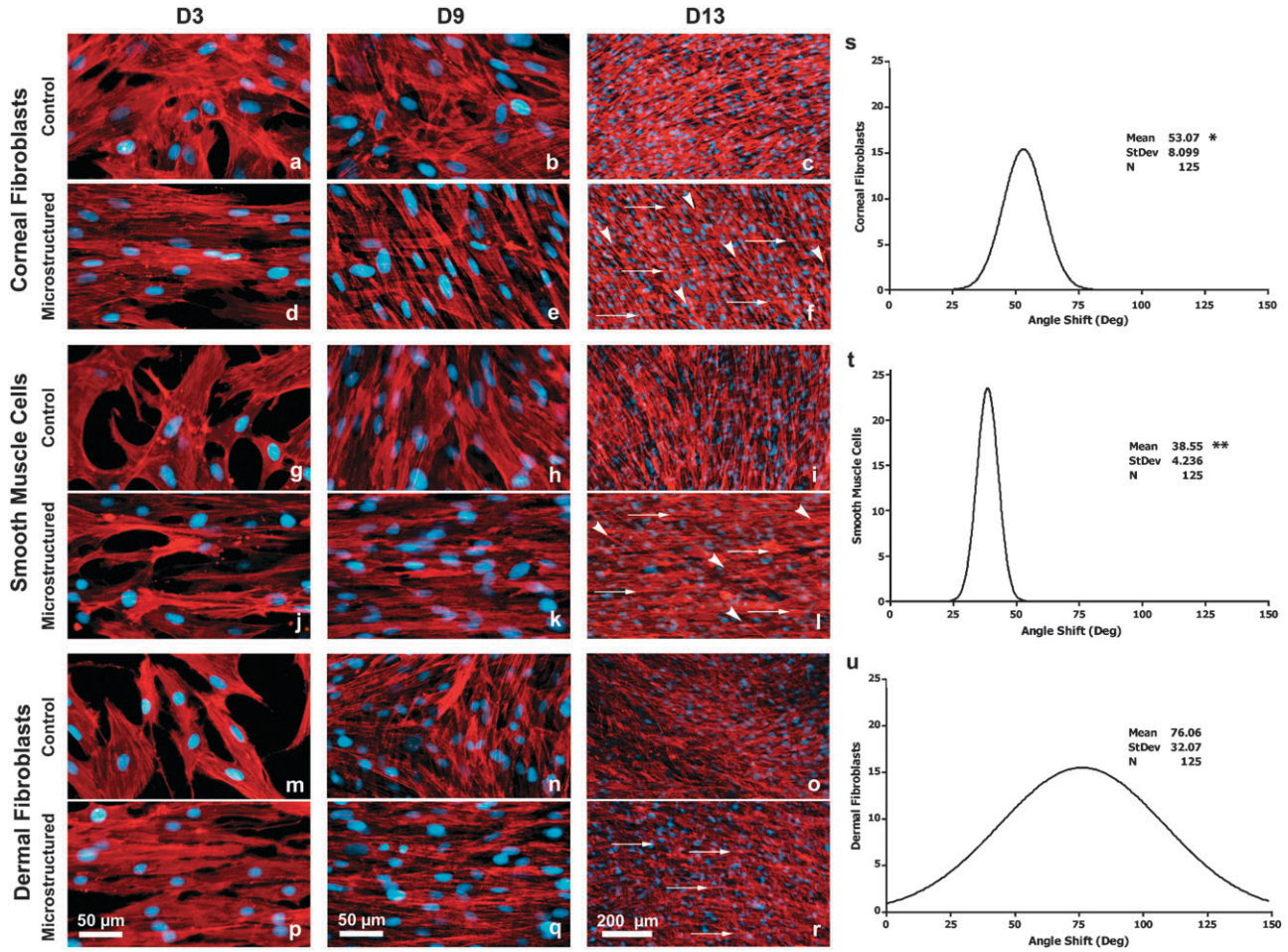

Fig. 2 Immunofluorescence staining of actin filaments of corneal fibroblasts, smooth muscle cells and dermal fibroblasts cultured on SEBS substrates. Corneal fibroblasts grown on microstructured SEBS show that cells are confluent in the bottom monolayer and aligned with the gratings, the second cell layer is oriented with a characteristic angle shift from the bottom layer as we can observe at day 9 and day 13, which can not be found in control samples (**a**–**f**). Smooth muscle cells are also aligned with the gratings and have a specific orientation within their second cell layer at day 13, as opposed to the control where we can observe random cell distribution (**g**–**l**). For dermal fibroblasts, the orientation is unidirectional on the bottom layer and shows no specific orientation on the second layer, dermal fibroblasts grown on control sample show no sign of orientation (**m**–**r**). Gratings have a 4 µm period and a 1 µm linewidth. Normal distribution of angle shift measured for each cell type has been performed. The second layer of corneal fibroblasts displayed a 53.07 ± 8.1 degree shift from the first cell layer (**s**), whereas smooth muscle cells' second layer angle shift was 38.55 ± 4.24 degrees (**t**). The dermal fibroblasts' angle shift was 76.06 ± 32.07 degrees (**u**), suggesting that this cell type does not organize in a specific configuration. Results showed a significant difference ($p < 0.05$) between each groups, clearly demonstrating that angle shift is cell type dependant. * indicates that corneal fibroblasts' angle shift is significantly different than the one of smooth muscle cells and dermal fibroblasts. ** indicates that smooth muscle cells' angle shift is significantly different than the one of dermal fibroblasts.

fibroblasts on microstructured SEBS self-assembled in an organized manner of alternating oriented collagen layers as they do *in vivo* in a corneal stroma.[27]

Interestingly, the surface topography induced cells and csECM organization in a particular spatial pattern specific for each cell type. Such a pattern gave rise to the internal organization of the 3D engineered-tissue since there is no biomaterial added with the self-assembly approach. Human corneal fibroblasts responded to microstructured SEBS by orienting themselves and the csECM they produced in consecutive cell–csECM layers with a 60 degree shift from the previous underlying layer. This spatial structure is similar in organization to lamellae found in the normal cornea *in situ*.[1] SMC presented a similar response to microstructured substrates although the angle shift was 30 degrees, which is similar to the native human SMC media arrangement.[28] This aspect of the tissue structure is of critical importance since optical[1] and mechanical[29] properties depend on cell and ECM orientation.

It is obvious that functional properties such as transparency[30] or compliance are of the utmost importance in these tissues. Therefore, these findings should represent a significant advantage for producing tissue-engineered organs for transplantation. Local spontaneous spatial organization of csECM has been observed before in cell cultures[31] but it was not controlled and occurred over small surface area of a few microns. Organization of a first cell–ECM layer was also observed by contact guidance using grating patterns allowing cells to penetrate the grooves.[32] Those models prevent the important cell–ECM interactions that allow for the 3D

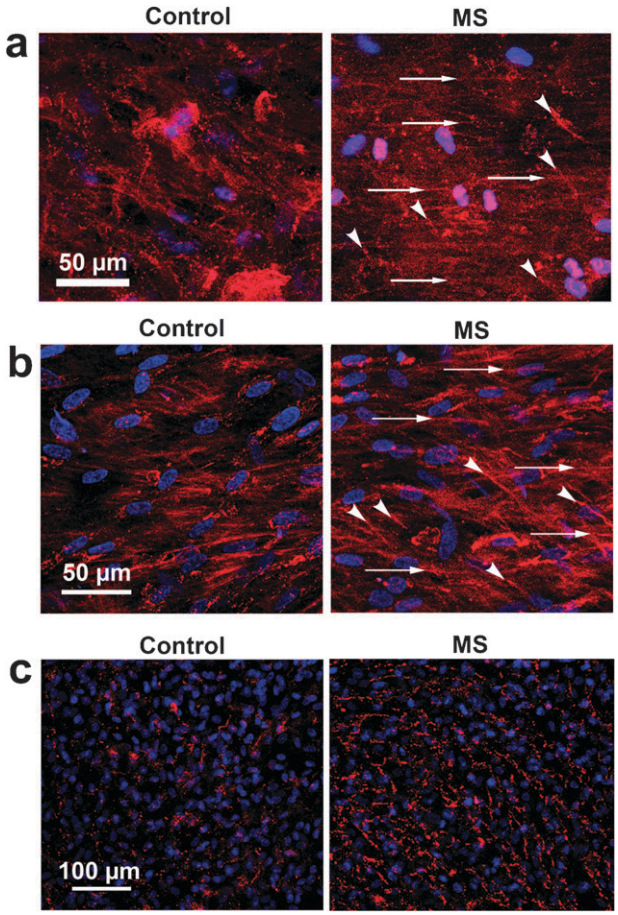

Fig. 3 Confocal imaging of corneal fibroblasts, smooth muscle cells and dermal fibroblasts csECM on microstructured and flat SEBS. Type I collagen fibers are shown in red, cells nuclei in blue, the arrows represent collagen from the bottom layer and the arrowheads collagen fibers from the top layer. Human corneal fibroblasts grown on flat SEBS substrates (control) show no signs of csECM structural orientation. Same cells grown on microstructured (MS) SEBS samples reveal that csECM have an organization similar to the one observed in cells (**a**). Immunofluorescence staining of type I collagen in SMC sheets revealed the same observation (**b**). Immunofluorescence staining of dermal fibroblast csECM shows type I collagen fibers. The control shows very little cross-linked type I collagen fibers and MS samples do not indicates the presence of collagen fibers orientation (**c**).

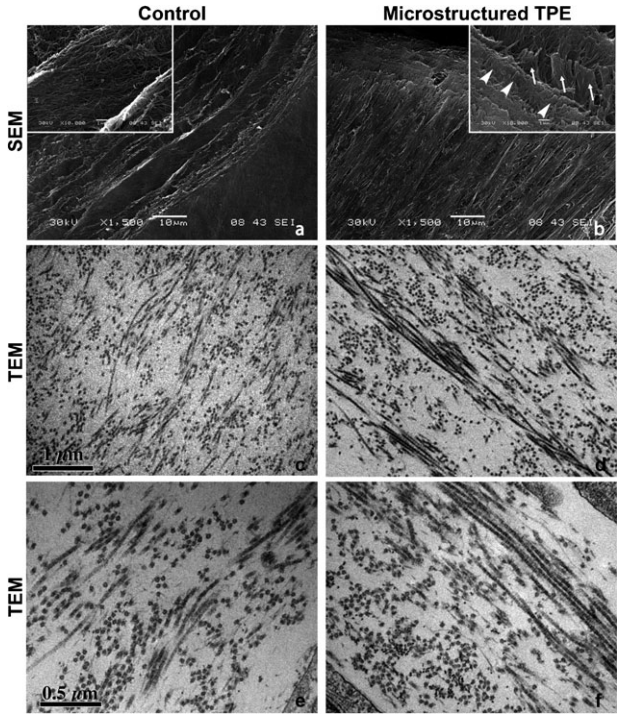

Fig. 4 Electron microscopy images of corneal fibroblasts on flat (control) and microstructured SEBS. The *x*–*y* plane SEM images of a control sample (**a**) shows different layers of collagen without any preferred orientation as opposed to the microstructured sample (**b**) where the csECM has many layers of oriented collagen. Insets in (**a**) and (**b**) show a higher magnification of the anisotropic and oriented superposed collagen layers of a single cell sheet. Arrows and arrowheads are showing different layers of oriented collagen within the reconstructed stroma. The *x*–*y* plane of TEM images of the control sample at 15 000× (**c**) and 30 000× (**e**) show no organization of the collagen layers. In the samples grown on microstructured SEBS we can see in (**d**) at 15 000× that many collagen layers are organized as in a native corneal stroma and in (**f**) at 30 000× we see 2 collagen layers and a corneal fibroblast. In TEM images, the dots are representing collagen fibers perpendicular to the *x*–*y* plane and striated lines are collagen fibers running in a parallel direction of the *x*–*y* plane.

structural organization of the tissue, and thus did not achieve cell–ECM organization for more than one layer. The platform developed in the present work allows for the 3D (*x*, *y* and *z*) spatial organization of the entire substitute over large surface area, which is consistent with the production of a tissue engineered substitutes produced for transplantation. In fact, since cells and ECM are oriented within the entire sample surface area of the SEBS sample, the oriented tissue sizes only depends on the dimension of the microstructured SEBS culture substrates, and this could be as large as 300 cm^2.

Tissue functionality

In order to evaluate whether the production of organized consecutive layers of cell–csECM obtained with microstructured SEBS would improve tissue functionality, we took advantage of the self-assembly approach described previously[7,22] to produce human living corneal and dermal substitutes and TEVM. For corneal substitutes, transparency is one of the main challenges in tissue engineering and among the most important properties of this organ. Control corneal substitutes were produced using our conventional culture technique[6,7] and oriented corneal substitutes were produced on microstructured SEBS, following the same culture technique steps. Both control and microstructured corneal substitutes are comprised of 2 stacked tissue sheets, and seeded with epithelial cells. Control tissue-engineered corneal substitutes were translucent since a paper letter underneath could be readily observed. However, the same types of substitutes grown on microstructured SEBS clearly revealed a better transparency than the control (Fig. 5a). In order to quantify the transparency levels of both tissues produced using microstructured or control conditions, we analyzed both samples with a spectrophotometer (Fig. 5a). Transparency of the microstructured corneal substitutes was improved over the

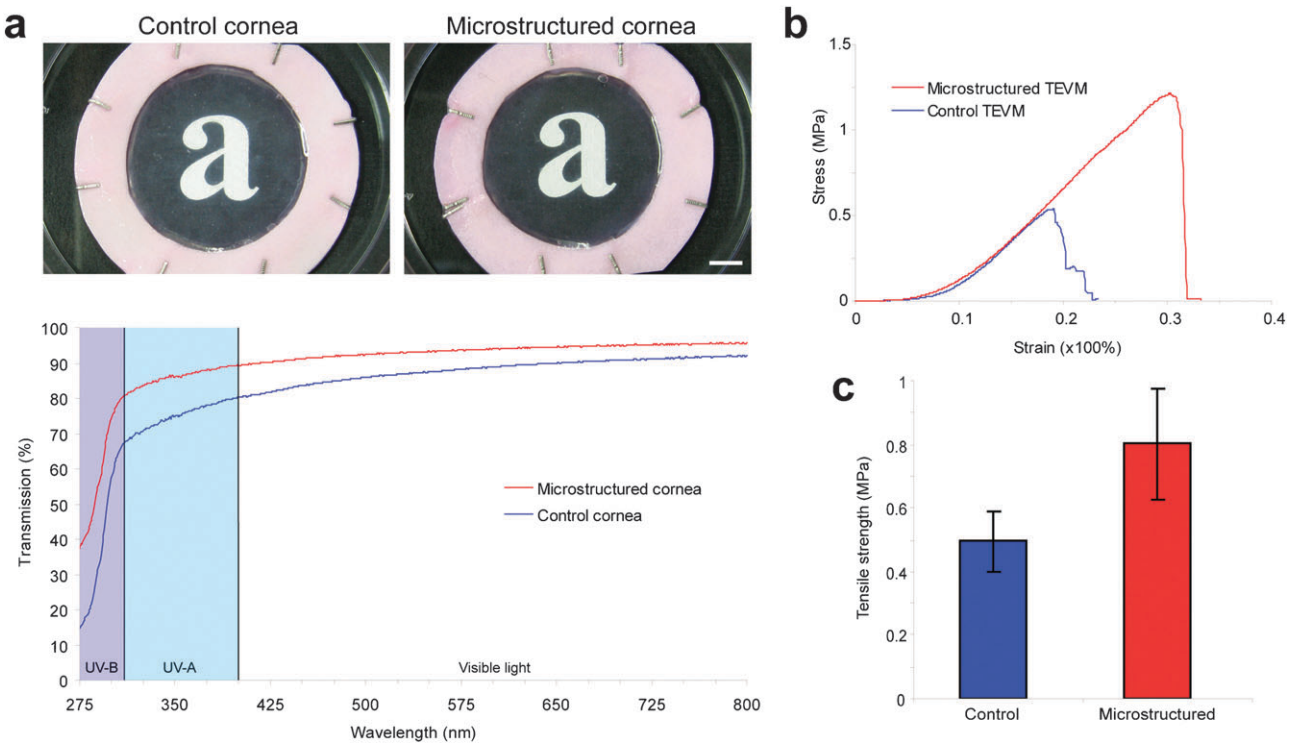

Fig. 5 Tissue functionality analyses. Corneal substitutes have been cultured on control and microstructured substrates. Microstructured samples exhibit a better transparency as we can observe on the macroscopic view and on the transmission spectrum measurement, scale bar 5 mm (**a**). Stress–strain curves of TEVM show that microstructured samples have improved mechanical properties when they are circumferentially aligned inside tissue-engineered substitutes compare to the non-organized substitutes, strain is expressed as a percentage of deformation (**b**). The tensile strength of dermal fibroblast sheets are slightly improved when they are cultured on microstructured substrates compare to flat substrates (**c**). Representative curves of transmission and stress–strain with a statistically significant difference for each condition.

entire visible spectrum, and we observed an 11% increase in transparency at 400 nm compared to the control. The thickness of the control cornea was 49 ± 11 μm and for the microstructured cornea 54 ± 7 μm, with no significant statistical difference. For vascular media substitutes, smooth muscle cell sheets grown on microstructured or control substrates were rolled onto a mandrel following a circumferential alignment. We then performed uniaxial tensile strength testing on 5 mm ring section of the substitutes to assess the mechanical properties of the TEVM (Fig. 5b). The microstructured TEVM presented a 2-fold increase in their mechanical strength compared to the control TEVM. Dermal fibroblast sheets presented a slight increase in the tensile strength measured following the longitudinal axis of the microstructured samples, compared to control dermal fibroblasts sheets (Fig. 5c).

The improved functionality obtained with tissue-engineered corneal substitutes, produced with highly organized stroma compared to randomly oriented control stroma, is consistent with the regular collagen alignment responsible for the adequate function of the native corneal stroma. Also, these results emphasize how it is possible to recreate the organization of a native corneal substitute *in vitro*, an organization which contributes to its transparency.[33,34] Human blood vessels are also known to be functionally dependant of their internal structural organization. Our model underlines the importance of organization in TEVM with improved mechanical properties, an aspect of critical importance for the development of tissue-engineered blood vessel. Dermal fibroblast sheets grown over a microstructured substrate had only a slight improvement in mechanical properties over the control. This is consistent with the poor organization of collagen fibers in tissue produced on microstructured substrates as well as in native tissue.

Conclusions

In this paper, we established the feasibility of producing highly-organized 3D tissue-engineered substitutes comprising an ECM featuring physiological density and organization. By culturing on microstructured SEBS using the self-assembly approach of tissue engineering, we achieved the alignment of the first layer of cells and csECM that resulted in the subsequent regular organization of the cell layers growing on top of them. In addition, the angle shift between consecutive cell–csECM layers varied with the type of mesenchymal cells that mimicked *in vitro* the organization of their respective native tissues. Most importantly, this improvement in the organization of the internal tissue structure resulted in improved functionality of tissue-engineered human corneal, vascular media and dermal substitutes. Hence, our results emphasize that the tissue origin of the cells plays a significant role in the properties of the reconstructed tissues, and suggest that it is preferable to use cells of the same origin than the tissue to engineer. Moreover, in addition to constituting a significant step towards the production

of improved organs by tissue engineering for clinical applications, this contact guidance approach also provide models for experimental studies such as the understanding of pathways and identification of signaling/ECM molecules involved in the production of highly organized tissues.

Acknowledgements

The authors would like to thank D. Larouche for help in figure preparation and C. Roberge for useful comments during the preparation of the manuscript. The authors would also like to thank Richard Janvier for the preparation of specimen for electron microscopy. We also thank the Réseau de Recherche en Santé de la Vision from the FRSQ. This work was supported by a joint collaborative program between The National Research Council of Canada grant no NRC-66473 and the Canadian Institutes of Health Research grant no MOP-53170.

References

1 P. M. Pinsky, D. van der Heide and D. Chernyak, *J. Cataract. Refract. Surg.*, 2005, **31**, 136–145.
2 F. S. Fay and C. M. Delise, *Proc. Natl. Acad. Sci. U. S. A.*, 1973, **70**, 641–645.
3 G. A. Ksander, L. M. Vistnes and E. H. Rose, *Plast. Reconstr. Surg.*, 1977, **59**, 398–406.
4 J. Bush, M. W. Ferguson, T. Mason and G. McGrouther, *J. Plast. Reconstr. Aesthet. Surg.*, 2007, **60**, 393–399.
5 R. Langer and J. P. Vacanti, *Science*, 1993, **260**, 920–926.
6 F. A. Auger, F. Berthod, V. Moulin, R. Pouliot and L. Germain, *Biotechnol. Appl. Biochem.*, 2004, **39**, 263–275.
7 N. L'Heureux, S. Paquet, R. Labbe, L. Germain and F. A. Auger, *FASEB J.*, 1998, **12**, 47–56.
8 T. S. Girton, V. H. Barocas and R. T. Tranquillo, *J. Biomech. Eng.*, 2002, **124**, 568–575.
9 S. Guido and R. T. Tranquillo, *J. Cell Sci.*, 1993, **105**(Pt 2), 317–331.
10 M. Zhao, A. Agius-Fernandez, J. V. Forrester and C. D. McCaig, *Invest. Ophthalmol. Vis. Sci.*, 1996, **37**, 2548–2558.
11 G. Grenier, M. Remy-Zolghadri, D. Larouche, R. Gauvin, K. Baker, F. Bergeron, D. Dupuis, E. Langelier, D. Rancourt, F. A. Auger and L. Germain, *Tissue Eng.*, 2005, **11**, 90–100.
12 G. Grenier, M. Remy-Zolghadri, F. Bergeron, R. Guignard, K. Baker, R. Labbe, F. A. Auger and L. Germain, *Tissue Eng.*, 2006, **12**, 3159–3170.
13 S. N. Bhatia, U. J. Balis, M. L. Yarmush and M. Toner, *FASEB J.*, 1999, **13**, 1883–1900.
14 E. E. Endler, P. F. Nealey and J. Yin, *J. Biomed. Mater. Res., Part A*, 2005, **74**, 92–103.
15 D. M. Brunette, *Exp. Cell Res.*, 1986, **164**, 11–26.
16 C. Oakley and D. M. Brunette, *J. Cell Sci.*, 1993, **106**(Pt 1), 343–354.
17 A. I. Teixeira, P. F. Nealey and C. J. Murphy, *J. Biomed. Mater. Res., Part A*, 2004, **71**, 369–376.
18 C. J. Bettinger, B. Orrick, A. Misra, R. Langer and J. T. Borenstein, *Biomaterials*, 2006, **27**, 2558–2565.
19 E. Vrana, N. Builles, M. Hindie, O. Damour, A. Aydinli and V. Hasirci, *J. Biomed. Mater. Res., Part A*, 2008, **84**, 454–463.
20 A. F. Laplante, L. Germain, F. A. Auger and V. Moulin, *FASEB J.*, 2001, **15**, 2377–2389.
21 L. Germain, F. A. Auger, E. Grandbois, R. Guignard, M. Giasson, H. Boisjoly and S. L. Guerin, *Pathobiology*, 1999, **67**, 140–147.
22 P. Carrier, A. Deschambeault, M. Talbot, C. J. Giasson, F. A. Auger, S. L. Guerin and L. Germain, *Invest. Ophthalmol. Vis. Sci.*, 2008, **49**, 1376–1385.
23 A. I. Teixeira, G. A. Abrams, P. J. Bertics, C. J. Murphy and P. F. Nealey, *J. Cell Sci.*, 2003, **116**, 1881–1892.
24 J. D. Glawe, J. B. Hill, D. K. Mills and M. J. McShane, *J. Biomed. Mater. Res., Part A*, 2005, **75**, 106–114.
25 S. Gerecht, C. J. Bettinger, Z. Zhang, J. T. Borenstein, G. Vunjak-Novakovic and R. Langer, *Biomaterials*, 2007, **28**, 4068–4077.
26 L. Meier and E. D. Hay, *J. Cell Biol.*, 1975, **66**, 275–291.
27 Y. Komai and T. Ushiki, *Invest. Ophthalmol. Vis. Sci.*, 1991, **32**, 2244–2258.
28 M. K. O'Connell, S. Murthy, S. Phan, C. Xu, J. Buchanan, R. Spilker, R. L. Dalman, C. K. Zarins, W. Denk and C. A. Taylor, *Matrix Biol.*, 2008, **27**, 171–181.
29 S. Kalath, P. Tsipouras and F. H. Silver, *Ann. Biomed. Eng.*, 1986, **14**, 513–524.
30 D. Kaplan and F. A. Bettelheim, *Biochim. Biophys. Acta*, 1972, **279**, 92–101.
31 X. Guo, A. E. Hutcheon, S. A. Melotti, J. D. Zieske, V. Trinkaus-Randall and J. W. Ruberti, *Invest. Ophthalmol. Vis. Sci.*, 2007, **48**, 4050–4060.
32 A. Pietak, A. McGregor, S. Gauthier, R. Oleschuk and S. D. Waldman, *J. Tissue Eng. Regen. Med.*, 2008, **2**, 450–453.
33 D. M. Maurice, *J. Physiol.*, 1957, **136**, 263–286.
34 J. L. Cox, R. A. Farrell, R. W. Hart and M. E. Langham, *J. Physiol.*, 1970, **210**, 601–616.

